Aerodynamics of Long Fibres Settling in Air at 10 < *Re* < 100

Guo Q. QI, Graham J. NATHAN and Richard M. KELSO

School of Mechanical Engineering and Centre for Energy Technology, The

University of Adelaide, Adelaide SA 5005 AUSTRALIA

Email: guo.qi@adelaide.edu.au

Abstract

The aerodynamics of long aspect ratio nylon fibrous particles has been investigated experimentally whilst settling in air under super dilute conditions without any influence of secondary flows and at fibre Reynolds numbers of 10-100 based on fibre length. Measurement of the orientations and velocities of fibrous particles is undertaken by two-dimensional Particle Tracking Velocimetry (PTV), based on the two end-points. A statistical evaluation of fibres' mean vertical and horizontal components of settling velocities, angular velocity, orientation, number density is presented and used to assess particle aerodynamics.

Keywords: Sedimentation; aerodynamics; PTV; fibrous particle

1 Introduction

One approach to reduce the use of fossil fuels is their partial substitution with biomass, or organic matter, which is a renewable and more environmentally "friendly" resource for energy supply. Such fuels can be derived from trees, agricultural residues and other plants. The percentage of biomass being used is increasing around the world for these reasons. However biomass is fibrous and there is a paucity of data describing the aerodynamics of fibrous particles. In order to increase the efficiency of the combustion of biomass, the aerodynamics of biomass particles needs to be investigated.

The settling motion of a particle is a basic class of its motion. The settling motion of a fibrous particle is much more complex, and more poorly understood than that of a sphere. A sphere settles in a purely vertical direction. However for a fibrous particle, the instantaneous horizontal drift cannot be neglected. A fibrous particle also exhibits rotation. A large number of previous investigations have studied the hydrodynamics of fibres under the conditions of relevance to the paper making industry. But these conditions differ from those in combustion. Theoretical treatments include the slender body theory by Batchelor [1] and the concentration instability by Koch and Shaqfeh [2]. Experimental investigations include that of Metzger *et al* [3], Herzhaft and Guazzelli [4], Salmela, *et al* [5], Herzhaft *et al* [6]. Previous numerical investigations were performed by Shin *et al* [7], Butler and Shaqfeh [8], Lin and Zhang [9], Lin *et al* [10], Kuusela *et al* [11], Kuusela, *et al* [12], Tornberg and Gustavsson [13], Shin *et al* [14]. Previous investigations to study the drag coefficient of fibrous particles were performed by Gabitto and Tsouris [15], Fan *et al* [16], McKay *et al* [17], Unnikrishnan and Chhabra [18], Haider and Levenspiel [19], and so on. The conditions under which these investigations were performed are summarized in Table 1. However none of these investigations provide detailed measurements of a bulk settling fibres in the range of $10 < Re_L < 100$ (fibre's Reynolds number based on its length).

Koch and Shaqfeh [2] studied theoretically the instability of a dispersion of sedimenting spheroids and pointed out that hydrodynamic interactions between sedimenting fibres give rise to an increase in the number of neighbouring particles in the vicinity of any given particle. They suggested that the suspension is unstable to particle number density fluctuations. They also argued that the convective motion (cluster formation) may lead to an average sedimentation velocity which is larger than the maximum possible value for a particle in a quiescent fluid. This theory can be verified by accurate measurements of settling

velocity and orientation of fibres.

Clift *et al* [20] reported that, for a single fibrous particle Reynolds number $Re_d > 0.01$(based on its diameter), a cylinder falls with its axis oriented horizontally and exhibits steady motion with this orientation up to Re_d of order 100. However, this is yet to be extended to a cloud of interacting particles in suspension. Salmela *et al* [5] experimentally studied the settling of dilute and semi-dilute fibre suspensions for $0.0003 < Re_L < 9$ in a liquid. At $Re_L \sim O(1)$, for small volume fractions $\Phi < 0.0005$ they found that fibres settle with their long-axis preferentially in the horizontal state and the settling velocity and the fluctuation of settling velocity increases with Φ. They also found that the steady-state settling velocity has a maximum that exceeds the velocity of an isolated particle because of a change in average orientation of the fibres from horizontal to vertical. With $\Phi > 0.0005$, fibres settle preferentially with their long-axis aligned with the direction of gravity, i.e. the average orientation gradually changes from horizontal state to vertical. However, from Table 1 it can be seen that, for a bulk settling of fibres of $Re_L \sim O(10)$ and $Re_L \sim O(100)$, no similar investigations seem to be available.

Herzhaft and Guazzelli [4] and Metzger *et al* [3] experimentally investigated sedimenting suspensions of fibres with $Re_L \approx 0.0001$, also in a liquid. For this case, the inertia acting on the fibrous particles approaches zero, causing the fibres to tend to align with the direction of gravity for dilute and semi-dilute suspensions. This contrasts the case of $Re_L \sim O(1)$ where fibre orientations are horizontal. Herzhaft and Guazzelli [4] pointed out that their experiment demonstrates the existence of an instability but could not confirm whether or not the argument of Koch and Shaqfeh [2] is correct. Herzhaft and Guazzelli also assessed the influence of a fibre's aspect ratio. They found that the aspect ratio has little influence on the

fibre's orientation and that the dimensionless settling velocity is much smaller for long fibre than for short one. Although this regime is different from that of Salmela *et al* [5], Herzhaft and Guazzelli [4] also found in their experiment that the settling velocity can be larger than the Stokes' velocity of an isolated vertical fibre in dilute suspension. Further, with increasing volume fraction, the fluctuation of settling velocity and fibres' orientation anisotropy was found to increase. The cause of this correlation deserves further investigation.

Kuusela *et al* [11] simulated the settling of spheroids under steady state sedimentation at $0.5 < Re_L < 3.5$. The authors assessed the role of aspect ratio of fibres and found the maximum settling velocity to decease with increasing aspect ratio. They also found that the volume fraction of peak velocity increases with increased volume fraction. These results are in good agreement with Herzhaft and Guazzelli's work [4]. They found an orientational transition of the spheroids is characterized by enhanced number density fluctuations. They predicted the orientation distribution that arises from a competition between inertial forces acting on individual particles and hydrodynamic interactions between particles. For super dilute systems, inertial effects tend to align fibres to a horizontal position whereas in sufficiently concentrated systems the interactions tend to align the fibres with gravity. Around the transition from a horizontal to vertical orientation, the mean settling velocity increases with increasing of Φ to a maximum that may even exceed the terminal settling velocity of a single spheroid. These accord with the experimental results of Salmela *et al* [5]. However like the work of Salmela *et al* [5], see Table 1, the Re_L of this investigation was limited to less than 3.5.

Butler and Shaqfeh [8] performed a numerical simulation of inhomogeneous sedimentation of rigid fibres in the limit of zero of Re_L. Their simulation revealed that the steady settling

velocity increases with the number density of fibrous particles simulated in the dilute regime. The predictions of orientation distribution agreed with the experimental result of Herzhaft and Guazzelli [4], i.e. the particles have a most probable orientation that is close to vertical. Furthermore the simulation showed that the orientation of fibrous particles tend to be more vertical with increasing of number density in the dilute regime. However this assessment is yet to be extended to higher Reynolds number.

Table 1 presents a summary of all previous measurements of settling slender particles. It can be seen that there have been 4 experimental and 4 numerical investigations. From the Table we can see there are 3 main features of present work compared with previous work. The first is that for bulk settling fibres, the present Reynolds number in the range of $10< Re_L < 100$ has not been investigated. The second is that the fluid phase of the present work is air, so the ratio of particle density to fluid is two orders of magnitude higher than that of previous work. The third is that the ratio of facility dimension to particle's length of the present work is 310, so there is no influence of secondary-flow in the settling chamber.

In the light of above review, we seek to further the understanding of the aerodynamics of settling fibrous particles in the range of $Re_L = 10 – 100$, with for a range of volumetric loading and with no boundary limitation. As can be seen from Table 1 these conditions have yet to be reported previously. Therefore, the aim of the present work is to use the novel method developed in Qi *et al* [21] to measure the velocity and orientation of a fibrous particle simultaneously and to investigate the aerodynamics of these fibres, notably their distribution of settling velocity, horizontal velocity and orientation. We also aim to identify the relationship between settling velocity, orientation, angular velocity and volume fraction, and relationship between settling and horizontal velocity and orientation.

Table 1 Comparisons between present and previous work

Authors	***L*** **(mm)**	***L/d***	**Fluid phase**	Re_L	**(*Φ*),** $n_p(L/2)^3$	ρ_{fp}/ρ_f	**Facility dimensions (mm)**				**Method**
							length	**width**	**height**	**Width/*L***	
Present Work	2	40	Air	10-100	(<0.0001) <0.03	958.3	650	620	2000	310	PTV
Salmela *et al* [5]	2.3, 5	23, 50	Water, glycerin, oil	0.0004-9	(0.0004-0.5)	2.25, 2.62	100	100	N/A	20	Real time digital image
Herzhaft and Guazzelli [4]	0.5-1.1	5, 11, 20, 32	Water	< 0.0001	0.001-1.0	2.1	65	35	400	32	Real time digital image
Fan *et al* [16]	1.5-7	4,6,19, 22,37	Water, glycerin	0.4-100 (Re_d)	Single particle	1.2, 8.0	Diameter 187			27	Real time digital image
Metzger *et al* [3]	1.5-2.1	10,13, 16,44	Liquid	0.0004	0.1,0.2, 0.3,0.7,1	1.1, 8.5	200	40	100	19	PIV
Butler and Shaqfeh [8]	N/A	11	N/A	<0.00001	0.154	N/A	Length : width : height 1:1:2 1:1:8				Numerical Simulation
Kuusela et al [11]	N/A	1,3,5,7	N/A	0.5-3.5	(0.001-0.1)	2.5				32	Numerical Simulation
Tornberg and Gustavsson [13]	N/A		N/A	<0.00001	25, 50, 100 fibres	N/A	Length : width : height 2:2:8 2:2:4				Numerical Simulation
Shin [7]	N/A	2.3-10	N/A	0-10.6	(<0.0057), <0.09	N/A	N/A				Numerical Simulation

2 Experimental apparatus/facility

Only a brief description of the experimental apparatus and approach is provided here, with details presented by Qi *et al* [21]. Fig. 1 presents the orientation definition of a fibre. The plane of *x*-*y* is the image plane. The angle α (0°-90°) is defined to be the azimuth of a fibre and θ (0°-90°) its orientation.

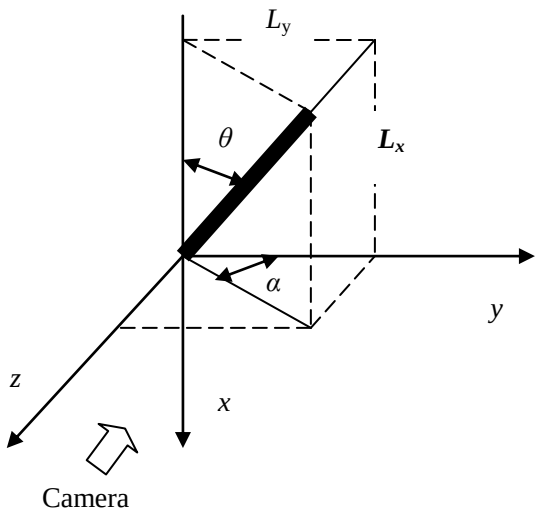

Fig. 1 The orientation definition of a fibre, *x*-*y* plane is the image plane.

Fig. 2 presents a schematic diagram of the experimental apparatus. The experimental method employed a typical Particle Tracking Velocimetry (PTV) technique. The laser used in the experiments was a Quantel Brilliant Twins double-cavity pulsed Nd: YAG 10 Hz laser.

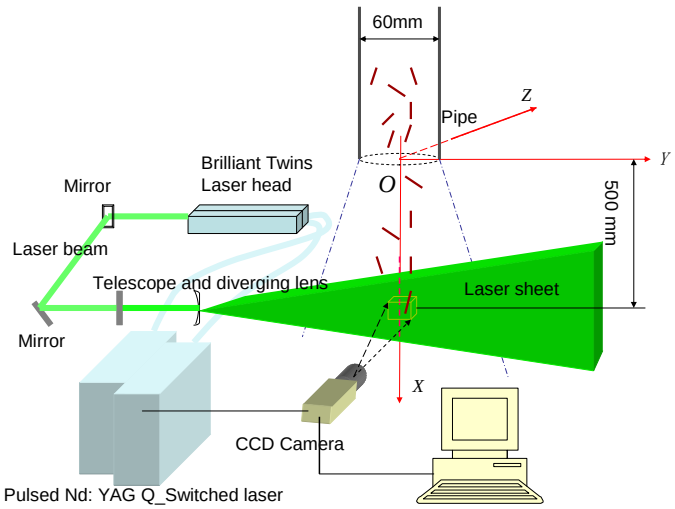

Fig. 2 Experimental arrangement (not to scale). The surrounding settling chamber (650mm×620mm cross section) is not shown for clarity.

The settling chamber was of nominally square cross section with a 650mm × 620mm, height of 2,000mm and was made of Perspex. The fibrous particles were introduced into the top of the chamber and settled over a distance of 2.5-3.0m through a 2,000 mm long pipe of 60mm diameter. Fibre's settling velocities were measured for settling distances of both 2.5m and 3.0m. The mean settling velocities obtained were identical for both cases, confirming that the fibres have reached their terminal settling velocities and steady state conditions. The intensity distribution of laser sheet is nearly Gaussian. This property is exploited to determine whether a fibre is fully or partly within the light sheet. This can be achieved by comparing the intensities of the signal at two endpoints of the fibre. Because of the Gaussian light sheet intensity distribution, a partly-in fibrous particle will exhibit a significant difference between the intensity values of the two endpoints. For a "full-in" fibrous particle, the intensity along the major axis of the fibre is nearly constant while for a part-in one, the intensity at the two endpoints differs significantly. Hence it is possible to discriminate by either comparing the intensity of two endpoints of the fibre, or by comparing the standard deviation of intensity along the major axis. If the standard deviation is less than the threshold,

it is a full-in fibrous particle. Full details of this approach are provided by Qi *et al* [21].

To measure the settling velocity and Φ, the volume fraction was controlled here to be in the range of volume fraction $\Phi \leq 0.0001$, which is a super dilute condition so that there were few particles that exhibited clumping. Hence the number density of fibrous particle in the viewing area (volume) was calculated by counting the number of particles, and the volume fraction was computed exactly. The coordinates of the two endpoints of each object (fibrous particle) were obtained. Since the length L of these fibres is constant, the spatial orientation θ of fibres was calculated by following trigonometric function:

$$\theta = (\arccos \frac{|x_{e2} - x_{e1}|R}{L}) \times (\frac{180}{\pi}) \quad (°), \qquad (1)$$

where R is magnification of camera image system; x_{e2} and x_{e1} are coordinates of x values of two endpoints.

Image pairs were recorded by the digital camera with a known time separation (Δt). After image processing the displacements of two endpoints of fibrous particles along the x and y axis can be obtained. From this $\boldsymbol{V}_{e1x}$, $\boldsymbol{V}_{e1y}$ and $\boldsymbol{V}_{e2x}$, $\boldsymbol{V}_{e2y}$ can be calculated by Eq. (2), as follows:

$$V_{e1x} = \frac{(x_{e12} - x_{e11})R}{\Delta t}, V_{e1y} = \frac{(y_{e12} - y_{e11})R}{\Delta t}, V_{e2x} = \frac{(x_{e22} - x_{e21})R}{\Delta t}, V_{e2y} = \frac{(y_{e22} - y_{e21})R}{\Delta t}, \qquad (2)$$

where V_{e1x} is the velocity of endpoint 1 in the x direction; V_{e1y} is the velocity of endpoint 1 in the y direction; V_{e2x} is the velocity of endpoint 2 in the x direction; V_{e2y} is the velocity of endpoint 2 in the y direction; x_{e12} is the x axis coordinate of endpoint 1 from the second image, x_{e11} is the x axis coordinate of the endpoint 1 from the first image; y_{e12} is the y axis coordinate of the endpoint 1 from the second image and so on. A fibre's centroid velocity V_{cx} = 1/2 (V_{e1x}+V_{e2x}) and V_{cy}=1/2(V_{c1y}+V_{c2y}) represents the vertical and horizontal components of

settling velocities, respectively. Since data are obtained from an image pair, the orientation of a fibrous particle equals the average orientation from the first and second images:

$$\theta = \frac{1}{2}(\theta_1 + \theta_2), \quad (3)$$

$$\theta_1 = \arccos \frac{|x_{e21} - x_{e11}|R}{L} \times (\frac{180^\circ}{\pi}), \quad (4)$$

$$\theta_2 = \arccos \frac{|x_{e22} - x_{e12}|R}{L} \times (\frac{180^\circ}{\pi}), \quad (5)$$

$$\alpha_1 = \arccos \frac{|y_{e21} - y_{e11}|R}{L\sin\theta_1} \times (\frac{180^\circ}{\pi}), \quad (6)$$

$$\alpha_2 = \arccos \frac{|y_{e22} - y_{e12}|R}{L\sin\theta_2} \times (\frac{180^\circ}{\pi}). \quad (7)$$

The angular velocities (rad/s) of a fibre are defined to be:

$$\omega_{vertical} = \frac{(\theta_1 - \theta_2) \times (\frac{\pi}{180})}{\Delta t}, \quad (8)$$

$$\omega_x = \frac{(\alpha_1 - \alpha_2) \times (\frac{\pi}{180})}{\Delta t}. \quad (9)$$

3 Experimental results and discussions

3.1 Influences of volume fraction on vertical component of settling velocity of fibrous particles

Fig. 3 presents the dependence of $\overline{V_{cx}}$ on the volume fraction Φ for both the present work and previous work on logarithmic axes. The present measurements were conducted in the super dilute condition (0.1×10^{-5} – 10×10^{-5}). About 6000 runs were performed and the volume fraction for image was calculated by post-processing. The data point corresponding to the lowest volume fraction in Fig. 3 represents the case of one isolated particle per image, while the highest volume fraction is 98 fibres per image. Each data comes from the average

of each volume fraction in Fig 3, 4 and 5. It can be seen that $\overline{V_{cx}}$ increases monotonically with Φ. It is also clear that the present data is consistent with the trends in previous measurements with the differences attributed to the substantial differences in conditions, notably in Reynolds number and density ratio, but also in aspect ratio and confinement for some cases. The present work represents the first detailed assessment of this influence in the dilute regime.

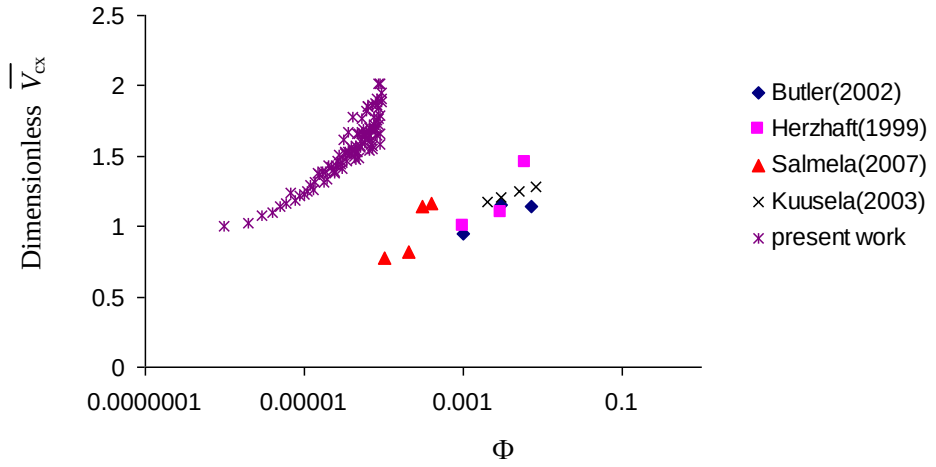

Fig.3 A comparison between the measured settling velocity of present and previous work, The measured mean settling velocity V_{cx} is normalised relative to the mean terminal settling velocity of an isolated particle, V_{ts}. See Table 1 for full details in experimental conditions.

3.2 Influences of volume fraction on orientation of fibrous particles

Fig. 4 compares the present measurements of orientation with previous work. It can be seen that $\overline{\theta}$ decreases with Φ, i.e. the fibrous particles tend to become more horizontal with decreasing Φ. This result can explain why the value of $\overline{V_{cx}}$ increases with Φ. An increase in Φ causes the fibre's major axis to tend to be more vertical, causing $\overline{V_{cx}}$ to increase, due both to a lower projected area and to increased aerodynamic interaction between vertically

aligned particles. From the figure we can also see, in all cases, that the orientations of the fibrous particles tend to become more vertical with increasing Φ. The present work is in the range $Re_L \sim O(10)$; while Salmela [5] and Kuusela [11] was in the range $Re_L \sim O(1)$; Herzhaft and Guazzelli [4] and Butler and Shaqfeh [8] belong to $Re_L \sim O(0)$. From the figure it can be seen that there are some difference in range of orientation transition across the three orders of magnitude Re_L regimes. For $Re_L \sim O(10)$, an increase in Φ causes settling fibres' orientation transition to vary from about 85° to 55°. That is, the settling fibres' orientations changes from horizontal state to a less horizontal one. For $Re_L \sim O(1)$, the settling fibres' orientations becomes increasingly vertical as Φ is increased (65° to 45°). Also for $Re_L \sim O(0)$, the settling fibres' orientations increases to become nearly vertical (45° to 25°). This agrees with Kuusela [11], who reported that the torque forcing a single fibre to become horizontally aligned is proportional to the Reynolds number of the fibre.

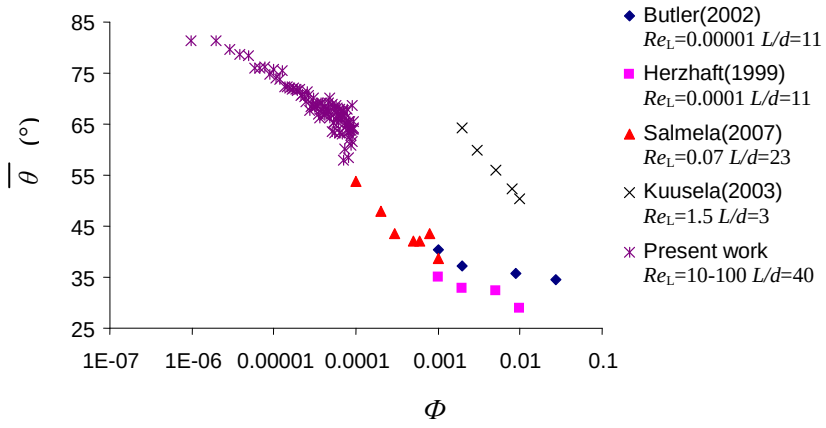

Fig. 4 A comparison of present and previous orientation measurements.

3.3 Influences of volume fraction on angular velocity component of fibrous particles

Because a fibre's change in orientation and azimuth can be measured over a time step Δt, the angular velocity ω can be calculated. In Fig. 5, the data come from the average of per volume fraction. Fig. 5 presents dependence on Φ of the two components of mean angular

velocity $\overline{\omega}_{vertical}$ and $\overline{\omega}_x$. It can be seen that $\overline{\omega}_{vertical}$ and $\overline{\omega}_x$ are both close to zero, indicating no preferred angular velocity, as expected. Also the scatter in $\overline{\omega}_{vertical}$ and $\overline{\omega}_x$ increase with Φ. It can also be seen that the RMS of $\overline{\omega}_{vertical}$, $\overline{\omega}_x$ is much more significant and also increases with Φ. These data show that the interactions between fibres, which increase with Φ, increase the tumbling and rotation of fibres, although with no preferred direction over this measurement range.

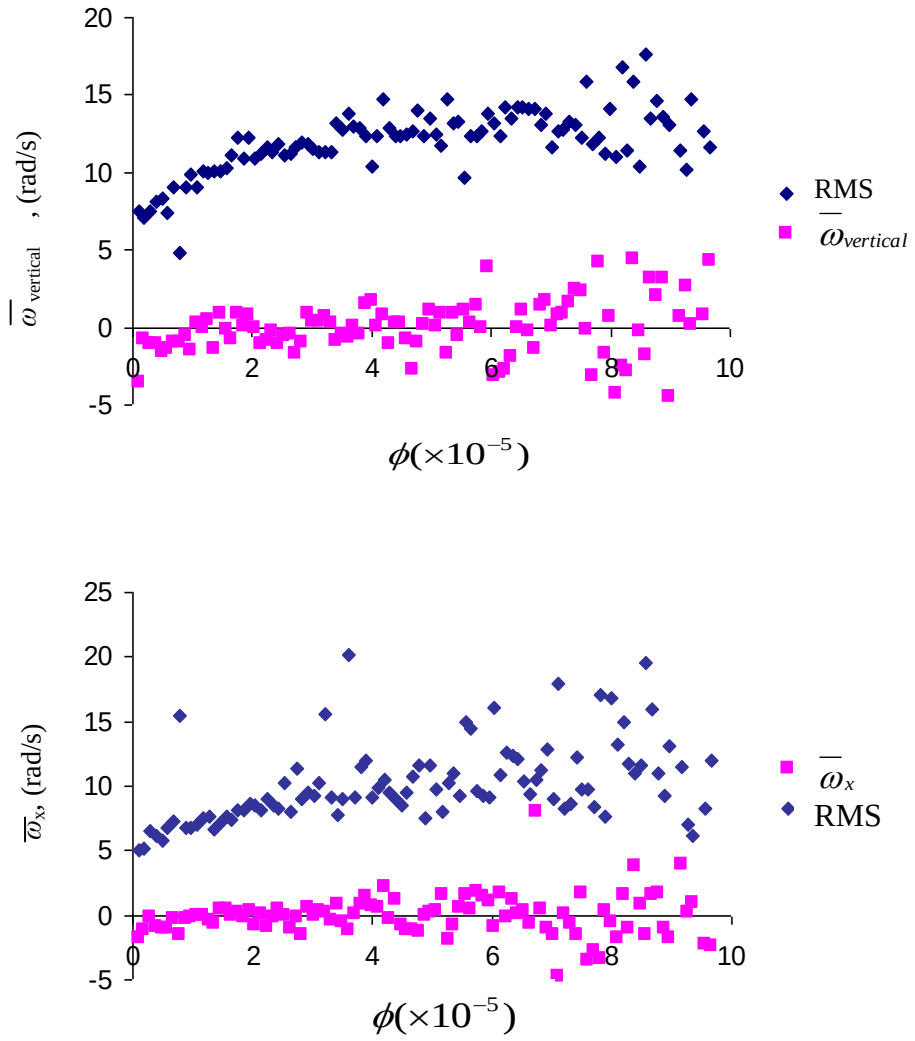

Fig. 5 The measured dependence on volume fraction, Φ, of $\overline{\omega}_{vertical}$ and $\overline{\omega}_x$.

3.4 Velocity and orientation distribution

Fig. 6 presents distribution of V_{cx} obtained from 29,364 samples for $\Phi < 9 \times 10^{-4}$. It can be seen that the mean settling velocity is about 0.75m/s with a skewness of 0.76 and kurtosis of -0.97.

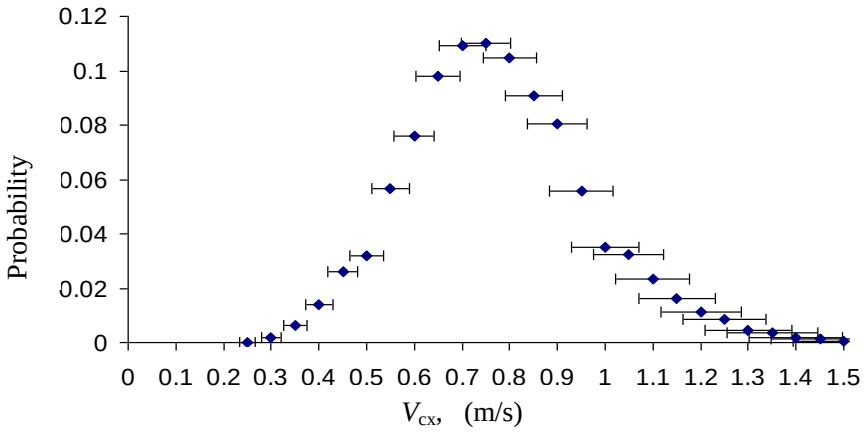

Fig.6 The measured distribution of settling velocity V_{cx}.

Fig. 6 indicates that there is no fundamental difference in the aerodynamic behaviour associated with the variation in straightness (refer to Qi *et al* [21] for measurement of straightness). Specifically no bimodality is evident, suggesting that there is no fundamental difference in the aerodynamics of perfectly straight and slightly curved fibres. That is the presence of a slight curve may increase the scatter in the velocity distribution but does not result in any fundamental change in aerodynamic behaviour. However, no comparable data is available against which to provide a quantitative assessment of the effect.

The motions of rotation, tumbling and swaying observed when fibrous particles settle in air induce a horizontal component of motion for fibres that does not occur with spherical particles. Fig. 7 shows the distribution of V_{cy} obtained from a sample size of 29,364. It can be seen that $\overline{V_{cy}}$ is approximately zero, showing that there is no preferred horizontal motion,

as expected. The standard deviation of distribution of V_{cy} is 0.07, which is approximately 9% of $\overline{V_{cx}}$, while the maximum value of V_{cy} is 0.2, which is approximately 30% of V_{cx}.

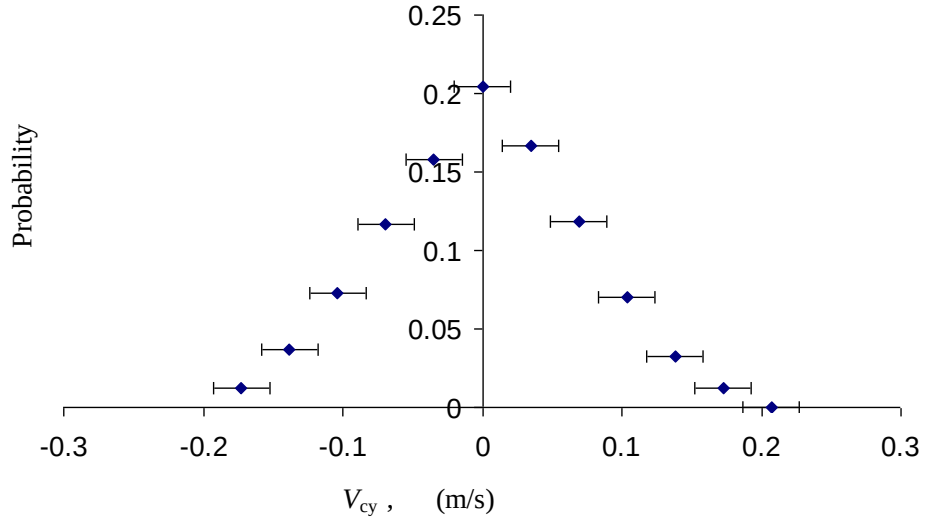

Fig. 7 The measured distribution of horizontal velocity V_{cy}.

Fig. 8 shows the orientation distribution of fibrous particles over the range of a volume fraction, $\Phi < 9\times10^{-4}$. It can be seen that the majority of fibres are broadly, but not exactly, horizontal. Indeed 88% of the fibres have an orientation of > 45°. This agrees with Clift *et al* [20] for a cylinder falling with its axis horizontal for $Re_d > 0.01$. Kuusela *et al* [11] argued that for $Re_L \sim O(1)$ sufficient torque is generated to change a fibre's orientation to horizontal. Nevertheless, there is significant departure from a truly horizontal orientation, with the most probable angle being 75° and with 0.2% of fibres being oriented at only 20° from the vertical direction.

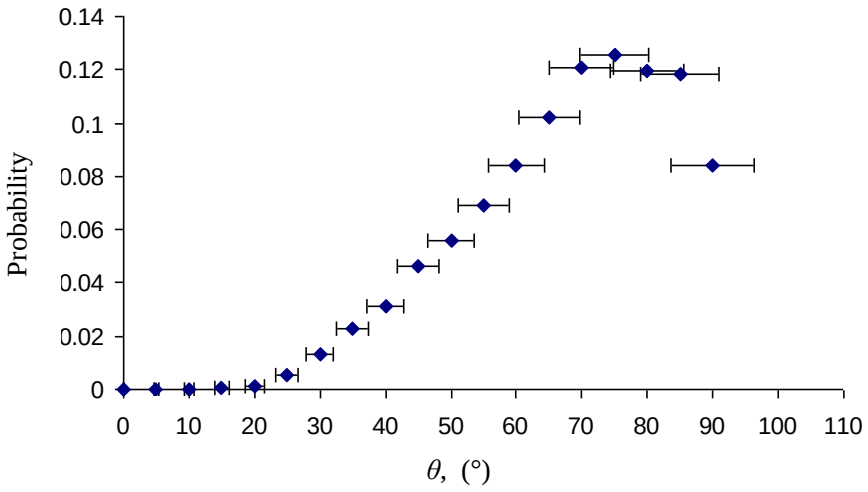

Fig. 8 The measured distribution of the orientation of the present fibrous particles from the vertical direction.

3.5 Relationship between $\overline{V_{cx}}$, $\overline{V_{cy}}$ and θ

In Fig. 9-10 the different orientations of fibres are presented for the sample size of 29,364 binned by orientation with increments of 5°. Here $\overline{V_{cx}}$ and $\left|\overline{V_{cy}}\right|$ are the average velocities for each bin. Fig. 9 shows that $\overline{V_{cx}}$ decreases linearly with θ for θ>30° but exhibits a complex behaviour for θ<30°. This shows that particles with a nearly vertical orientation have a slightly higher settling velocity than those with a more horizontal orientation, as expected, but the maximum difference is only 30%.

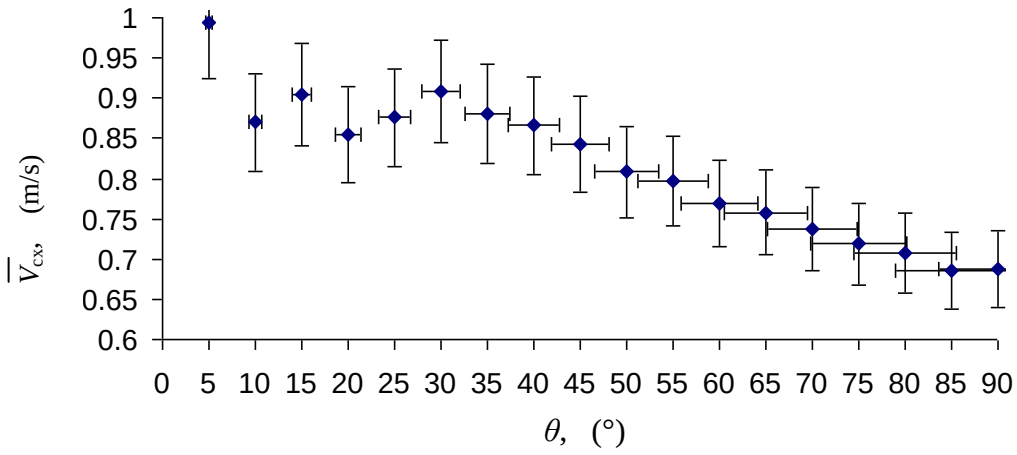

Fig. 9 The measured dependence of settling velocity, $\overline{V_{cx}}$, on orientation from the vertical direction, θ.

Fig.10 presents the relationship between $\left|\overline{V_{cy}}\right|$ and θ from the sample size of 29,364. It can be seen that this relationship can also be divided into the same two regions: $\theta < 30°$ and $\theta > 30°$. For small angles from the vertical direction, $\left|\overline{V_{cy}}\right|$ is highly sensitive to angle. The greatest horizontal velocity occurs for 0°-10°. For $\theta > 30°$, the horizontal component of velocity is non zero and only weakly dependent on θ. Interestingly $\left|\overline{V_{cy}}\right|$ is also non zero for $\theta = 90°$, showing that these particles are not stable, even for the most extreme cases in the data set. That is, no particles fall with a purely vertical motion and all exhibit some lateral motion, which is only weakly dependent on orientation. A slight maximum in $\left|\overline{V_{cy}}\right|$ occurs at 45°.

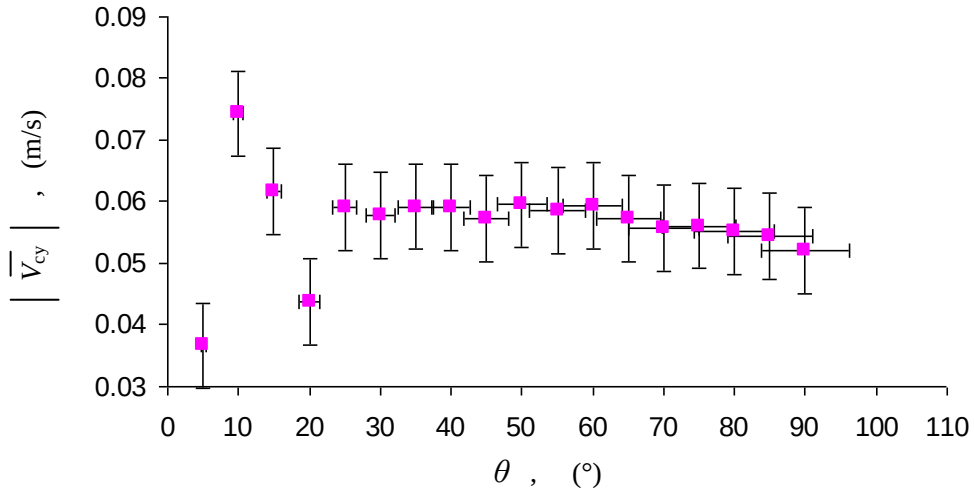

Fig. 10 Relationship between $|\overline{V_{cy}}|$ and θ.

3.6 Relationship between $|\overline{V_{cy}}|$ and azimuth (α)

In Fig.11 the different azimuth of fibres are presented for the sample size of 29,364 binned by orientation for increments of 10°. It can be seen that $|\overline{V_{cy}}|$ decreases linearly with α but is non zero at α = 90°. This indicates that, while the largest component is within the plane of the fibre, the component normal to it is 55% as large on average, because a horizontal fibre moving horizontally within its major axis plane has the minimum drag force. This shows that the motion of the fibre is highly three dimensional, and that the fibre does not simply tumble in a two-dimensional plane.

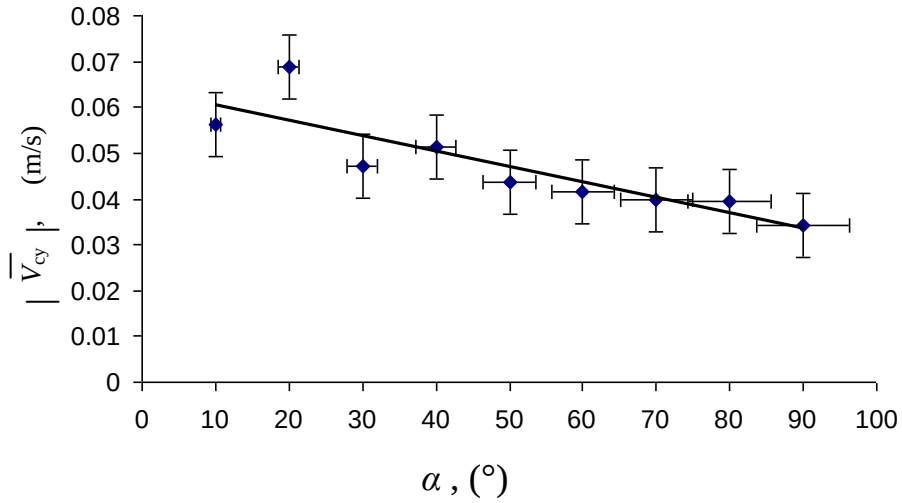

Fig. 11 The relationship between α and $\left|\overline{V_{cy}}\right|$.

4 Conclusions

The vertical components of settling velocities, angular velocity, orientation and number density of fibres settling in air with $Re_L \sim O(10)$ for volume fractions less than 9×10^{-4} are reported for the first time. It is found that the distribution of settling velocity is nearly Gaussian for these long aspect ratio fibres. Kuusela [11] and Herzhaft [4] argued that the aspect ratio has influences on settling velocity. The magnitude of $\overline{V_{cx}}$ is at maximum for vertical orientation and decreases nearly linearly with θ, the fluctuation of angular velocity increases with Φ, the directions of V_{cy} tend toward within the plane of the major axis of a fibre. The fibre's orientation tends to be more horizontal than that with $Re_L \sim O(1)$. Finally we find that these results qualitatively support the previous work under different regimes in finding that all the mean steady state settling velocities of fibres exceed the mean terminal settling velocity of a single fibre. This phenomenon is attributed to fibres' orientation transition from a horizontal to vertical state under super dilute conditions, which stems from increasing aerodynamic interactions between fibres.

Acknowledgement

This study has been supported by the Faculty of Engineering, Computer & Mathematical Science of The University of Adelaide and by an ARC Discovery Grant, both of which are gratefully acknowledged.

References

[1]G. K. Batchelor, Slender-body theory for particles of arbitrary cross-section in Stokes flow, Journal of Fluid Mechanics, Vol 44 (1970) 419-440.

[2] D. L. Koch and E. S. G. Shaqfeh, The instability of a dispersion of sedimenting spheroids, Journal of Fluid Mechanics, Vol 209 (1989) 521-542.

[3] B. Metzger, J. E. Butler and E. Guazzelli, Experimental investigation of the instability of a sedimenting suspension of fibre, Journal of Fluid Mechanics Vol 575 (2007) 307-332.

[4]B. Herzhaft, and E. Guazzelli, Experimental study of sedimentation of dilute and semi-dilute suspensions of fibres, Journal Fluid Mech, Vol 384 (1999) pp133-158.

[5] J. Salmela, D. M. Martinez and M. Kataja, Settling of dilute and semidilute fiber suspensions at finite Re, AIChE Journal, Vol.53 (2007) No.8

[6] B. Herzhaft, E. Guazzelli, M. B. Mackaplow and E. S. G. Shaqfeh, Experimental investigation of the sedimentation of a dilute fiber suspension, Physical Review Letters, Vol. 77 (1996) No. 2

[7] M. Shin, D. L. Koch and G. Subramanian, Structure of dynamics of dilute suspensions of finite-Reynolds number settling fibres, Physics of Fluids 21 (2009) 123304

[8] J. E. Butler and E. S. G. Shaqfeh, Dynamic simulation of the inhomogeneous sedimentation of rigid fibres, Journal Fluid Mech, Vol.468 (2002) pp205-237

[9] J. Z. Lin and L. Zhang, Numerical simulation of orientation distribution function of cylindrical particle suspensions. Applied mathematics and mechanics, 23(8) (2002) 906-912

[10] J. Z. Lin, Y. L. Wang, W. X. Wang and Z. S. Yu, Numerical simulation of the sedimentation of cylindrical pollutant particles in fluid. Journal Environ. Sci. 14(4) (2002) 433-438

[11] E. Kuusela, J. M. Lahtinen and T. Ala-Nissila, Collective effects in settling of spheroids under steady-state sedimentation, Physical review letter, vol 90 (2003) No 9.

[12] E. Kuusela, K. Hofler and S. Schwarzer, Computation of particle settling speed and orientation distribution in suspensions of prolate spheroids, J. Engineering Mathematics, 41 (2001) 221-235.

[13] A. K. Tornberg and K. Gustavsson, A numerical method for simulations of rigid fiber suspensions, J. Computational Physics, 215 (2005) 172-196.

[14] M. Shin, D. L. Koch D and G. Subramanian, A pseudospectral method to evaluate the fluid velocity produced by an array of translating slender fibers, Physics of Fluids 18 (2006) 063301.

[15] J. Gabitto and C. Tsouris, Drag coefficient and settling velocity for particles of cylindrical shape, Powder Technology 183 (2008) 314-322

[16] L. Fan, Z. Mao and C. Yang, Experiment on Settling of Slender Particles with Large Aspect Ratio and Correlation of the Drag Coefficient, Ind. Eng. Chem. Res. 43 (2004) 7664 - 7670.

[17] G. McKay, W. R. Murphy and M. Hillis, Settling characteristics of discs and cylinders, Chem Eng Res Des, Vol. 66 (1988)

[18] A. Unnikrishnan and R. P. Chhabra, An experimental study of motion of cylinders in Newtonian fluids: wall effects and drag coefficient, the Canadian Journal of Chemical Engineering, Vol. 69 (1991)

[19] A. Haider and O. Levenspiel, Drag coefficient and terminal velocity of spherical and nonspherical particles, Powder Technology, 58 (1989) 63-70.

[20] R. Clift, J. Grace and M. Weber, Bubbles, drops, and particles, ISBN 0-12-176950-X, Academic Press, New York, 1978

[21] G. Q. Qi, G. J. Nathan and R. M. Kelso, PTV measurement of drag coefficient of fibrous particles with large aspect ratio, Powder Technology, 229 (2012),261-269.